Wake and Surface Pressure Analysis of Vehicles in Platoon

Hesham Ebrahim, Robert Dominy

Northumbria University, Newcastle Upon Tyne, NE1 8ST, United Kingdom

Abstract

In this paper, the drag reduction benefits associated with 2 and 3 cars in platoon have been investigated. Following a validation of initial CFD simulations against experimental measurements, predictions of surface pressures and wake structure for alternative platoon configurations have been analysed to determine the changes of flow structure that influence the pressure field and drag force on each vehicle. Contrary to several publications it was found that in a platoon of two vehicles, the drag force of the trailing vehicle exceeded that of an isolated vehicle for close spacings. Analysis of this surprising result revealed that design features introduced to optimise the wake of an isolated vehicle can lead to a drag increase on a following vehicle. For three-vehicle platoons, the flow interaction between the leading and middle vehicles remained largely unchanged but the additional effect of the third vehicle resulted in all three vehicles exhibiting lower drag than that of an isolated vehicle. A clear implication of this work is that results from the analysis of vehicle platoons are likely to be sensitive to the geometry and wake structures of the chosen test vehicle which helps to explain why many previous studies have been seemingly contradictory.

1 Introduction

The concept of reducing road vehicle drag by harnessing the aerodynamic interference between closely spaced vehicles has acquired considerable attention in recent years due to the growing capabilities of vehicle autonomy and artificial intelligence (Davila et al., 2013), which have the potential to turn the concept into reality. The majority of cars currently being manufactured are already equipped with the systems required for safe operation in platoon such as inter-vehicle communication, automated braking and intelligent cruise control. Wider issues such as joining and leaving a platoon are under development and therefore it is possible that safe platoons could be on the road within the next five to ten years. Multi-vehicle platoons, have been a subject of fundamental research in an attempt to characterise the flow topology and to quantify the drag force initially using simple geometries. Authors have explored the potential of optimising the longitudinal spacing between thin circular disks (Morel and Bohn, 1980), cylindrical tubes (Ljungkrona and Sundén, 1993), a cylinder placed downstream of a flat disc (Koenig and Roshko, 1985) and an elliptical plate followed by a rectangular plate (Bull et al., 1996). These authors found that the highest drag reduction was when the spacing was optimised to allow for the development of a quasi-steady stable vortex that filled the inter-body cavity and allowed the separating free shear layers of the leading object, reattach onto the following object. This phenomena was successfully applied to industrial problems related to open train wagon partitions to invoke the formation of stable vortices (Saunders, Watkins, and Cassar, 1993), however, the transferability of a quasi-steady stable vortex to passenger vehicles is complicated due to the presence of a ground plane that removes the plane of symmetry or the stationary lower surface that a cavity relies on. Despite that, research in sport including bobsleigh crew members' position (Dabnichki and Avital, 2006), cycling team time trials (Blocken et al., 2018), cyclist followed by a motorbike (Blocken, Toparlar, and Andrianne, 2016) and marathon runners (Beves and Ferguson, 2017) have shown that drag reductions are plausible with careful development.

Similarly platooning in passenger vehicle aerodynamics has shown encouraging results with net drag reductions consistently demonstrated at $0.5L$ spacing and lower with the use of various vehicle geometries (Schito and Braghin, 2012). However, differences in the literature exist in regard to the highest drag saving vehicle in the platoon, which suggests that the individual vehicle's drag is sensitive to the platoon spacing and the type of geometry used. Early investigations on a 2-vehicle pair of minivans by Zabat et al. (1995) have reported that the vehicle experiencing the highest drag reduction was the trailing vehicle, before the phenomena reverses as the spacing is decreased below $0.5L$. It was also shown that the order of the highest drag saver differs for a 3-vehicle platoon. At spacings less than $< 0.5L$ the middle vehicle indicated the lowest drag followed by the leading and trailing vehicles respectively. For spacings above $> 0.75L$, the trailing vehicle showed the highest drag reduction followed by the middle and leading vehicles respectively. It is obvious that at close spacings complex changes occur to the flow-field that influence the drag, which they termed as the "strong interaction regime". Similar studies on notch-back (Altinisik, Yemenici, and Umur, 2015), idealised fast-back (Watkins and Vino, 2008) and idealised square-back (Le Good et al., 2019) geometries have shown that this behaviour is not universal and in fact the leading vehicle yielded the highest drag reduction, whilst the trailing vehicle exhibited detrimental drag (i.e. higher than in isolation) at some spacings in a 2 and 3-vehicle platoons. The latter study by Le Good et al. incorporated variations in slanted backlight angles including 0^o, 10^o and 25^o at $0.25L$ platoon spacing to determine the most efficient combination. They concluded that the "optimum" net drag reduction case was of 0^o, 25^o and 25^o combination, even though that the trailing vehicle experienced a drag higher than its isolation counterpart. A more comprehensive investigation of the influence of slant angles was by Pagliarella, Watkins, and Tempia (2007) on the Ahmed model geometry. They made force measurements along with surface pressure and wake surveys to quantify the platoon forces. It was found that the leading model base pressure increased due to the suppression of the trailing C-pillar and roll-up base vortices. This consequently reduced the drag force, whilst for the trailing vehicle the drag increased (above vehicle-in-isolation) predominantly due to the increase of forebody pressure from the leading model flow impingement. Other researchers including Browand and Hammache (2004) and Gheyssens and Van Raemdonck (2016) have reported the sensitivity of forebody geometry of basic trucks on drag through the use of small edge modifications. Browand and Hammache focused his analysis on 2-vehicle platoons and found that a rounded geometry followed by a blunt geometry yielded the highest net drag reduction. This resulted in significant drop in drag on the trailing vehicle in comparison to the leading vehicle. Similarly, Gheyssens and Van Raemdonck found a similar drag behaviour for a 3-vehicle platoon and reported that the middle vehicle had the lowest drag followed by the trailing and leading vehicles respectively, for spacings below $0.5L$. Overall, the majority of wind tunnel and road investigations of platoons focused on the measurement and reduction of drag to improve the fuel consumption efficiency, without characterising the changes associated with the flow topology and/or pressure field.

In general, platoon aerodynamics are difficult to test in wind tunnels due to the limited test section length required to accommodate a large number of vehicles without compromising the vehicles scale, which in turn influences the aerodynamic resolution and Reynolds number. CFD therefore offers a practical alternative to assess vehicles in platoon as demonstrated by several authors using RANS (Jacuzzi and Granlund, 2019) DDES (He et al., 2019) and DNS (Bruneau, Khadra, and Mortazavi, 2017). Both He et al. and Bruneau, Khadra, and

Mortazavi demonstrated the advantages of using higher order numerical solvers to determine time dependant flow features in platoon that are usually omitted by RANS that contribute to the vehicle's lateral instability. However, in terms of the averaged flow features that influence the mean drag measurements, the RANS solver has been shown to reproduce the wake structures and pressure field reasonably well for various aerodynamic studies including Bordei and Popescu (2011), Axerio et al. (2009), Soares, Garry, and Holt (2017), Fu et al. (2017), Maleki, Burton, and Thompson (2017) and Ebrahim, Dominy, and Leung (2016).

It is clear from the limited information in the literature, that simple geometrical changes such as the rear slant angle and front edge radius have a significant influence on the individual vehicle's performance and consequently on the platoon as a system. A disparity in the results reported previously with regard to the vehicle geometry that has the highest drag savings in relation to its position within the platoon and spacing remains vague and not well understood. The majority of the research reviewed was focused on idealised geometries or extremely bluff geometries such as trucks with only a few authors investigating representative passenger vehicle models. Therefore this work is aimed to apply validated computational methods to quantify the changes in flow-field and pressure distribution that lead to drag reductions on a production vehicle in platoon. It will also attempt to offer some insight into appropriate methods that could be used for development purposes of platoons.

2 Methodology

2.1 Experiments

2.1.1 The Wind Tunnel

The validation experiments were conducted in the Northumbria University wind tunnel which is a $^3/_4$ open jet, open circuit configuration (Figure 1), at a free-stream velocity of $V_\infty = 20ms^{-1}$ that corresponds to a Reynolds Number $Re_L = 1.5 \times 10^6$ based on the scaled model length.

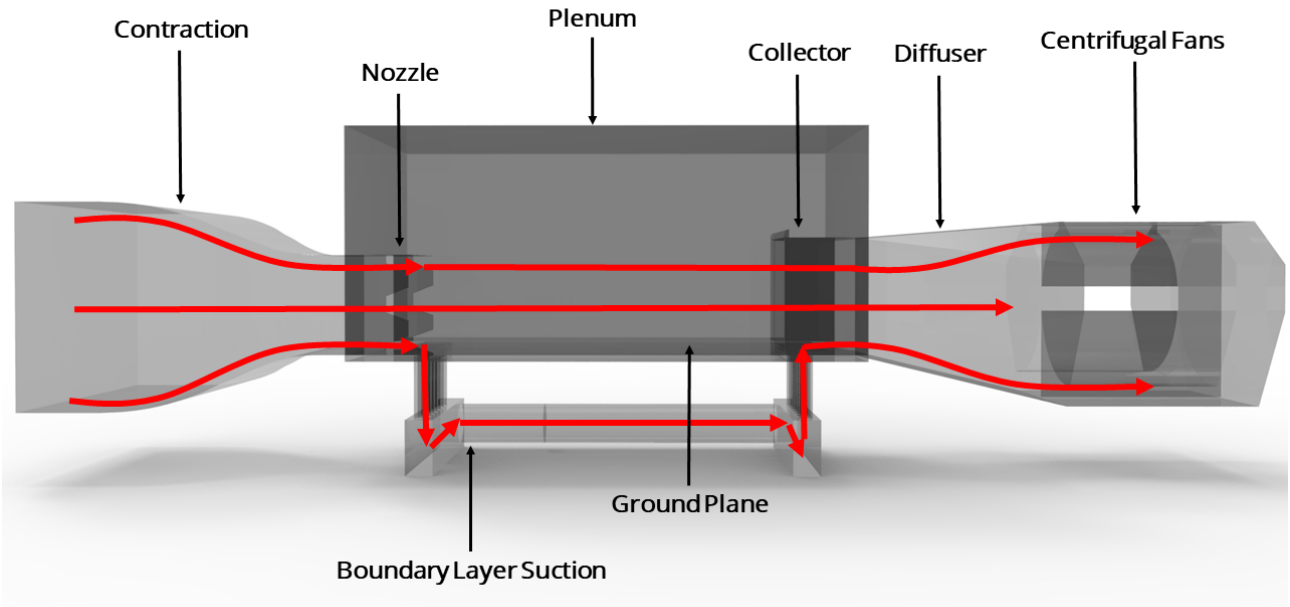

Figure 1: Northumbria University wind tunnel of $^3/_4$ open jet, open circuit configuration and its main components

The wind tunnel has a test section length of $L_T = 3.3m$ and a nozzle area of $A_N = 1.07m^2$ with an upstream boundary layer suction and a rolling road. For this investigation however, a fixed ground plane was adopted. The tests were conducted over the course of two weeks during which the atmospheric environment remained relatively stable. Pressure and temperature sensors distributed around the laboratory were monitored to ensure a consistent wind tunnel environment.

2.1.2 The Nissan Leaf

The entire study focused on quarter scale models of the 2016 model hatchback Nissan Leaf with the dimensions specified in Figure 2. The main aerodynamic features of this vehicle can be summarised as airflow-control headlights, sharply designed front fenders, rear lights and fenders, a large rear spoiler and clean underbody with a diffuser, which were all introduced to control the flow around the vehicle as explained thoroughly by Nakada, Ishikawa, and Oki (2014).

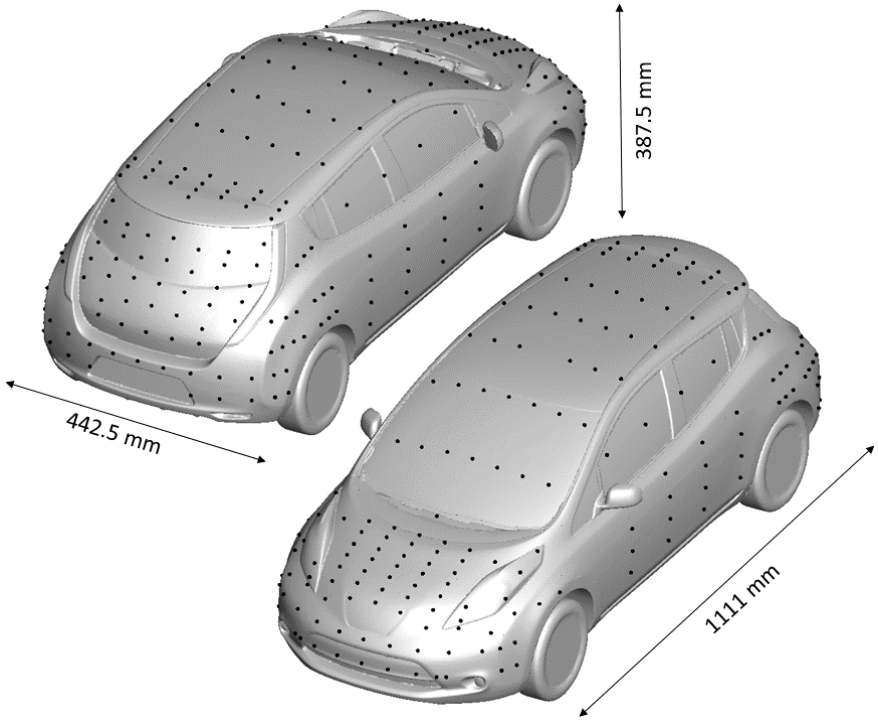

Figure 2: 1/4 Nissan Leaf 2016 scale model with 273 pressure tappings distributed on the entire vehicle

2.1.3 Pressure Measurement

The pressure acting on the vehicle was recorded using 273 pressure tappings with a finer distribution near the forebody and base surfaces (Figure 2). The taps are drilled normal to the surface and connected via flexible tubes to five 64-port pneumatic connections. Each group was sequentially connected to a 64-port miniature pressure scanner with a manufacturer quoted accuracy of $\pm 0.05\%$ of the full scale pressure range (i.e. 1kPa) to measure the pressure of the specified region. A conventional approach was used to define the pressure coefficients according to Equation 1 and the reference pressure was taken from a pitot-static probe mounted upstream of the test section nozzle that extends $100mm$ from the roof.

$$C_{Pi} = \frac{P_i - P_\infty}{0.5\rho_\infty V_\infty^2} \tag{1}$$

where P_∞ is the free-stream static pressure, ρ_∞ is the free-stream density and V_∞ is the free-stream velocity.

A pressure horizontal buoyancy correction as described by Mercker and Wiedemann (1996) was applied to the pressure measurements to account for the variation induced by the longitudinal displacement of the models inside an open-jet test section that is characterised by a variable pressure gradient according to Equations 2:

$$C_{Picorr} = C_{Pi,d} - C_{Pi,ideal} \tag{2}$$

where $C_{Pi,d}$ is the pressure coefficients measured at the displaced location of the model. $C_{Pi,ideal}$ is the pressure coefficients measured at the optimum location of the test section that equals to 1m from the jet in this case. For simplicity, the pressure was assumed symmetrical about the vehicle axis and only one side of the vehicle have been considered for the present study.

The probe locations shown in Figure 2 were interpolated using the inverse distance method to construct pressure maps that can be directly compared with the CFD simulations.

2.1.4 Force Measurement

The aerodynamic loads were recorded using a purpose built six-component internal force balance that consists of two parallel aluminium plates, one connected to the model and the other mounted to a rigid sting, in this case an overhead strut. Both plates are bridged by six strain gauge load cells attached directly to the rigid fixed plate and indirectly to the live plate via six thin rods of $1.6mm$ diameter. Table 1 summarises the characteristics of the six components force balance.

Load Cell Types	DS Europe SRL: 535 QD
Full Scale Load (FSL)	Up to $120N$
Repeatability	$\pm$0.02% FSL
Precision	$\pm$0.0033% FSL
Accuracy	$\pm$0.087% FSL

Table 1: Specifications of the six components force balance

For the present study, only the normalised drag was considered according to Equation 3:

$$C_{Xi} = \frac{F_X}{0.5\rho_\infty V_\infty^2 A} \tag{3}$$

where ρ is the free-stream air density, A is the projected model frontal area ($A = 0.145m^2$), V_∞ is the free-stream velocity. The drag coefficient was corrected for horizontal buoyancy using Equation 4:

$$C_{Xi_{corr}} = C_{Xi,d} - C_{Xi,ideal} \tag{4}$$

where $C_{Xi,d}$ is the drag coefficient measured at the displaced location of the model. $C_{Xi,ideal}$ is the drag coefficient measured at the optimum location of the test section that equals to 1m from the jet in this case.

2.2 Simulations

CFD simulations were carried out using Star-CCM+ with a computational domain that mimics the wind tunnel apparatus. The domain was discretised using a hexahedral grid topology and a prism layer refinement adjacent to the walls finely tuned to measure a $y+ \leq 1$ (as shown in Figure 3). This was primarily to avoid variation in the mesh topology, when comparing different turbulence models that require the $y+$ to be below a certain threshold. Sensitivity analyses were conducted in relation to the number of layers used close to the boundary as well as the first layer height, and it was found that the measurements were most accurate when 15 layers and a $y+ \leq 1$ was implemented.

A velocity inlet and a static pressure outlet were used to specify the wind velocity entry to exit direction. Stationary wall boundaries with slip conditions were applied to the top and side walls to inhibit shear stress calculations, whilst a fixed ground plane with a no-slip condition was used to replicate the ground condition of the wind tunnel floor.To ensure no large skewness was modelled in the mesh particularly in the area between the intersection of the stationary wheel and the static ground plane, a subtract function along with a contact patch function were used on both surfaces to prevent cells close to either boundary from collapsing and allow for the mesh to be modelled homogeneously. In addition, it is well known that in reality the relative movement between the ground and vehicle should be simulated with a moving wall, however, for this investigation, the inclusion of a moving wall did not influence the wake structure or pressure field significantly such that the conclusions of this study would no longer be relevant. A symmetry plane was chosen to halve the computational domain with the assumption that the flow is symmetrical about the vehicle axis. Following a mesh sensitivity analysis that indicated a negligible reduction of 0.6% of the drag after doubling the mesh size of 16 million cells, the adopted CFD settings to mimic the wind tunnel experiments are summarised in Table 2. Note, platoon configurations including the inter-vehicle spacing and Reynolds number were identical for the CFD and wind tunnel to allow for a direct comparison, including any vehicle simplifications made experimentally.

Initial investigations to determine the most accurate RANS model for platoons was undertaken using several turbulence models including k-ω SST, RNG and Realizable k-ϵ. The tests were conducted on idealised geometries to establish which turbulence model was capable of predicting the surface pressure, drag force and wake structures robustly on the leading and trailing models. The tests indicated that both the Realizable k-ϵ and k-ω SST were sufficient at predicting the flow features required, however, the k-ω SST resulted in inconsistencies in the wake structure found between CFD and wind tunnel measurements without optimising of the $a1$ coefficient that limits the calculated shear stress from exceeding a prescribed fraction of the turbulent kinetic energy. This was similar to the findings of Georgiadis and Yoder (2013) as they optimised the a1 coefficient to correlate the flow structure along a flat plate with experimental results to reduce the flow recirculation bubble separation.

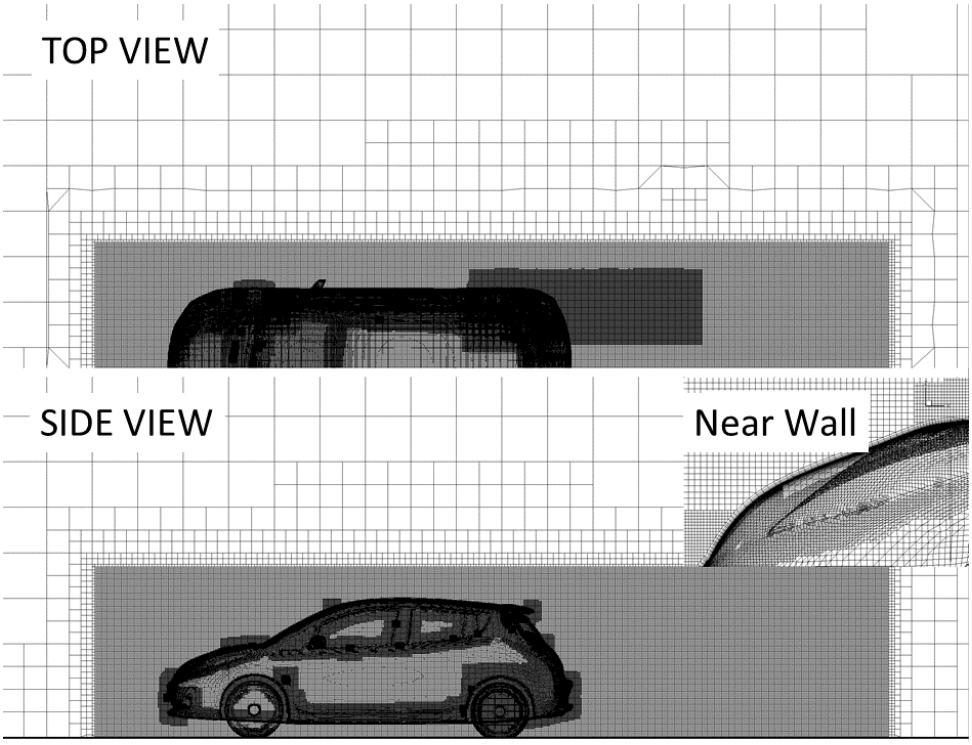

Figure 3: Nissan Leaf mesh topology

It was therefore decided to use the Realizable k-ϵ as it did not require any parameter to be optimised based on experimental measurements and the use of default values achieved reasonably accurate results.

In addition, an initial comparison between the Realizable k-ϵ model and an Improved Delayed Detached Eddy Simulation (IDDES) SST k-ω model showed only very small differences in terms of the time-averaged wake. The only significant advantages found in using a higher order model were the improved accuracy in capturing shear layer separations at critical backlight slant angles and in the availability of time histories that allowed for frequency and proper orthogonal decomposition (POD) analysis to characterise the unsteady flow-field (Ebrahim, 2019). However, for this study, the flow behind the vehicle was completely separated and rear surface separation points were clearly defined so for this particular investigation RANS offered a cheaper but reliable solutions.

In general, the flow-field around vehicles operating in a platoon is dictated by three-dimensional unsteady wake features that are caused by flow interference and high turbulence. The intensity of both parameters increase as the inter-vehicle spacing is reduced and therefore to capture the time-dependent flow dynamics accurately the use of unsteady simulation approaches is vital. However, for drag estimations, surface pressure trends and averaged flow features, Ebrahim, Dominy, and Leung (2016) showed that the Reynolds Averaged Navier-Stokes (RANS) is capable of producing reasonable results at the expense of small magnitude deviations in surface pressure and over-predictions of drag. The planes used for the investigations are shown in Figure 4.

Modelling Parameters	Adopted Settings
Reynolds Number	1.5×10^6
Mean Velocity	$20ms^{-1}$
Turbulence intensity	1%
Grid Topology	Trimmed hexahedral mesh
Number of Cells	Ranged from $15.7M$ to $40M$
Domain $(L_f/L_R/W/H)$	$3L/4L/3L/3L$
Near Wall Treatment	Hybrid all y+ mesh
Prism Layer Count	15 layers
First Cell Height	2×10^{-5}
Time	Steady State
Pressure/Velocity Coupling	Segregated flow
Equation of State	Constant Density
Viscous Regime	Turbulent
RANS Model	Realizable k-ϵ (RKE)

Table 2: Simulation settings for the platoon configurations

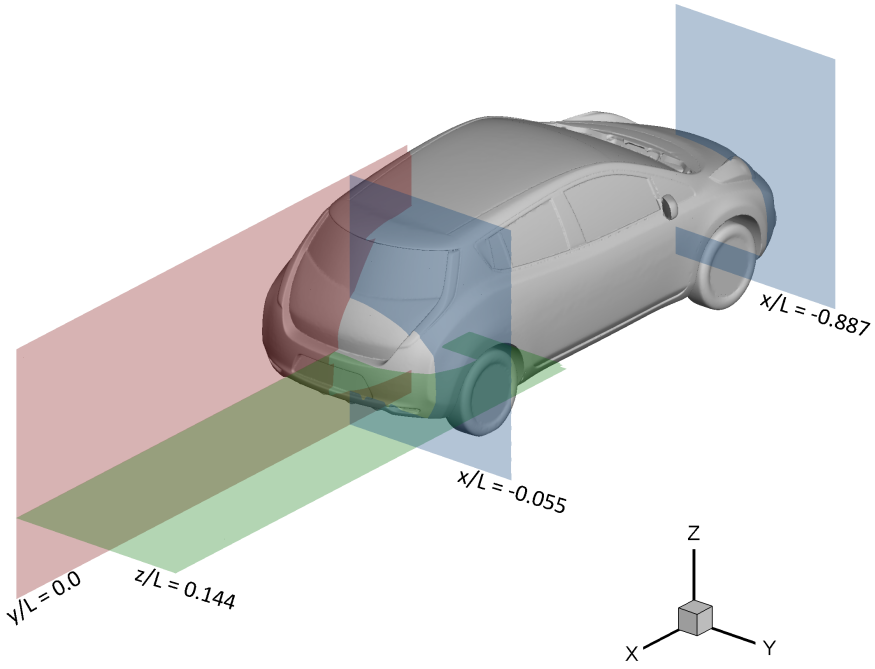

Figure 4: The planes used to investigate the wake structures

3 Results and Discussion

The results shown are only for the $0.0L$, $0.5L$ and $1.0L$ spacing. Additional simulations included $0.25L$ and $0.75L$ spacings, but for brevity there were not included in the following contour plots.

3.1 Single Vehicle

The CFD surface pressure results of the Nissan Leaf in isolation were validated against the wind tunnel measurements shown in Figure 5(a) for the forebody and Figure 5(b) for the base. It is evident that the CFD forebody and base pressures corresponded with the measured data and appeared logical for this vehicle geometry. The forebody pressure field indicates that the highest pressure was concentrated on the vehicle's leading edge with the pressure rapidly decreasing as the flow accelerates around the sharp front fenders, bonnet and headlights. Another region of high pressure was seen behind the cowl at the leading edge of the windscreen,

with the flow rapidly developing as the pressure decreases across the A-pillar and windscreen shallow curvature. Some discrepancies are seen in the pressure distribution of the wind tunnel measurements that were associated with the spatial resolution of the tappings in comparison to the CFD simulations. A more continuous pressure field was provided by the simulation due to the fine mesh, which distinguished areas of high pressure gradients around the A-pillars and fog lights that were not captured experimentally. In addition, the changes in base pressure field were determined with high accuracy, indicating that the flow is fully separated at the base. Peak pressure was localised below the spoiler where the flow recirculates and above the number plate. Lower pressure magnitudes were spotted close to the rear fenders suggesting fast moving flow in that region. A slight vertical misalignment was visualised in the exact location of the rear stagnation point (i.e. the point at which the wake collapses onto the base) between CFD and wind tunnel measurements, perhaps due to the distribution of pressure taps. In general, the RANS approach was able to predict the pressure field for an isolated Nissan Leaf with high precision and gives confidence in the near-wake structure produced.

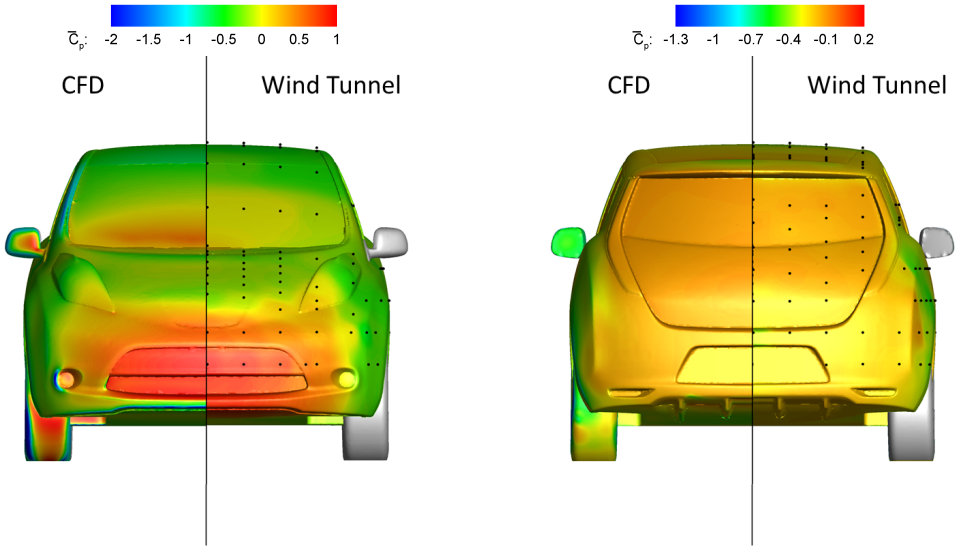

(a) Forebody C_P (b) Base C_P

Figure 5: Surface pressure coefficient comparison between the wind tunnel measurements and CFD for the Nissan Leaf

Assessment of the velocity magnitudes and in-plane velocity streamlines of a single vehicle as shown in Figure 6(a) reveals the near flow detachment characteristics behind the spoiler and along the upper base surface. The wake topology shows two counter-rotating C-pillar vortices, V1, centred at $y/L = \pm 0.08$ and fast moving flow underneath the diffuser section surrounded by low velocity gradients from the rear wheel wells flow separation. Figure 6(b) shows the centreline flow structure that is dominated by two counter-rotating vortices with their central cores diagonally misaligned. The upper vortex develops further downstream from the base due to the base angularity, whilst the bottom roll-up vortex occurs directly at the base behind the number plate. These recirculating zones are slightly under-estimated as a consequence of the simplifications made to the underbody, wheel wells and wheels. The wake closure point and vortex core locations are therefore modified from the production model shown by Nakada, Ishikawa, and Oki (2014). On the $z/L = 0.144$ plane in Figure 6(c) another two counter-rotating vortices form behind the side fenders with the in-plane streamlines marking a 45^o taper of the flow inboard. This low velocity wake rapidly develops and closes at $x/L = 0.1$.

Some of the main characteristics of the wake structure that were considered relevant to understanding the changes influenced by platooning were highlighted in Figure 6(a). These features include the central core position of the vortices as circular filled points and the symmetric lateral (or vertical in some cases) streamlines that link the vortex cores and closes the wake demonstrated as a filled spline. The vortex core positions and splines show the wake displacement, which is quite revealing in platoon, as a wider wake typically yields higher base pressures, which consequently reduces the drag coefficient. It also allows for direct comparison of the changes in averaged wake dynamics for different platoon spacings.

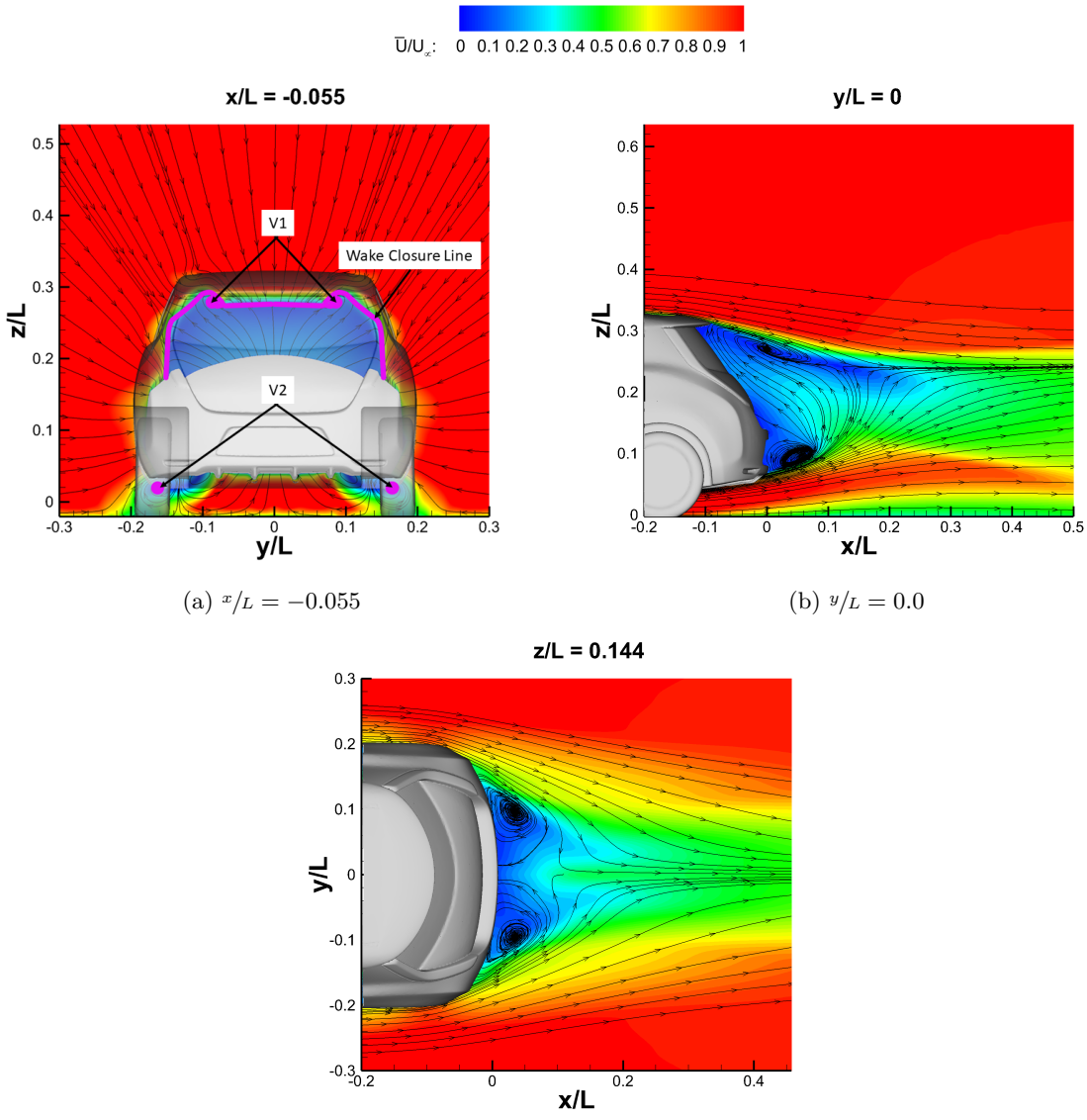

(a) $x/L = -0.055$

(b) $y/L = 0.0$

(c) $z/L = 0.144$

Figure 6: Velocity fields of the $x/L = -0.055$ plane (a), centreline plane (b) and vertical plane at $z/L = 0.144$ (c) with streamlines of the velocity in-plane components

3.2 2-Vehicle platoon

To further confirm the applicability of using the RANS methodology in predicting the expected flow features in platoon, an additional validation was conducted against the wind tunnel measurements for two platoon spacings of $0.0L$ and $0.5L$. The main pressure changes were seen to occur on the leading model base and the trailing model forebody similar to the findings of Altinisik, Yemenici, and Umur (2015), therefore only these regions were compared. Figure 7(a) and (b) demonstrate the correlation between the wind tunnel measurements and the CFD simulations for $0.0L$ and $0.5L$ spacings. Once again, the surface pressure topology captured by a limited grid of pressure tappings was less accurate than that acquired from the high spatial resolution of the simulation. CFD was able to finely render the pressure map interpolation to match the absolute pressure variations found using the tapped regions for both spacings. In Figure 7(a) a distinct increase in the leading model base pressure was found around the number plate that was not seen experimentally as no tappings occupied that region. For the trailing model forebody, the shift in stagnation point to the centre of the windscreen was captured. A localised pressure increase was also observed around the vehicle sides up to the headlights.

For larger platoon spacing of $0.5L$ as shown in Figure 7(b), the overall leading model base pressure magnitude appeared to have dropped (in comparison to $0.0L$ spacing), whilst the pressure acting on the trailing model forebody increased laterally. This pressure map trend proceeded to match that of $1.0L$ spacing in Figure 7(c) with the pressure magnitude being lower in larger areas of the bonnet, front side fenders and the upper portion of the windscreen. In general, a good agreement in pressure trend was seen between the two simulation environments, with minor over-prediction in the absolute pressure magnitudes by CFD. These variations are likely to be attributed to blockage effects and the intrusivity of the overhead strut that were not modelled computationally.

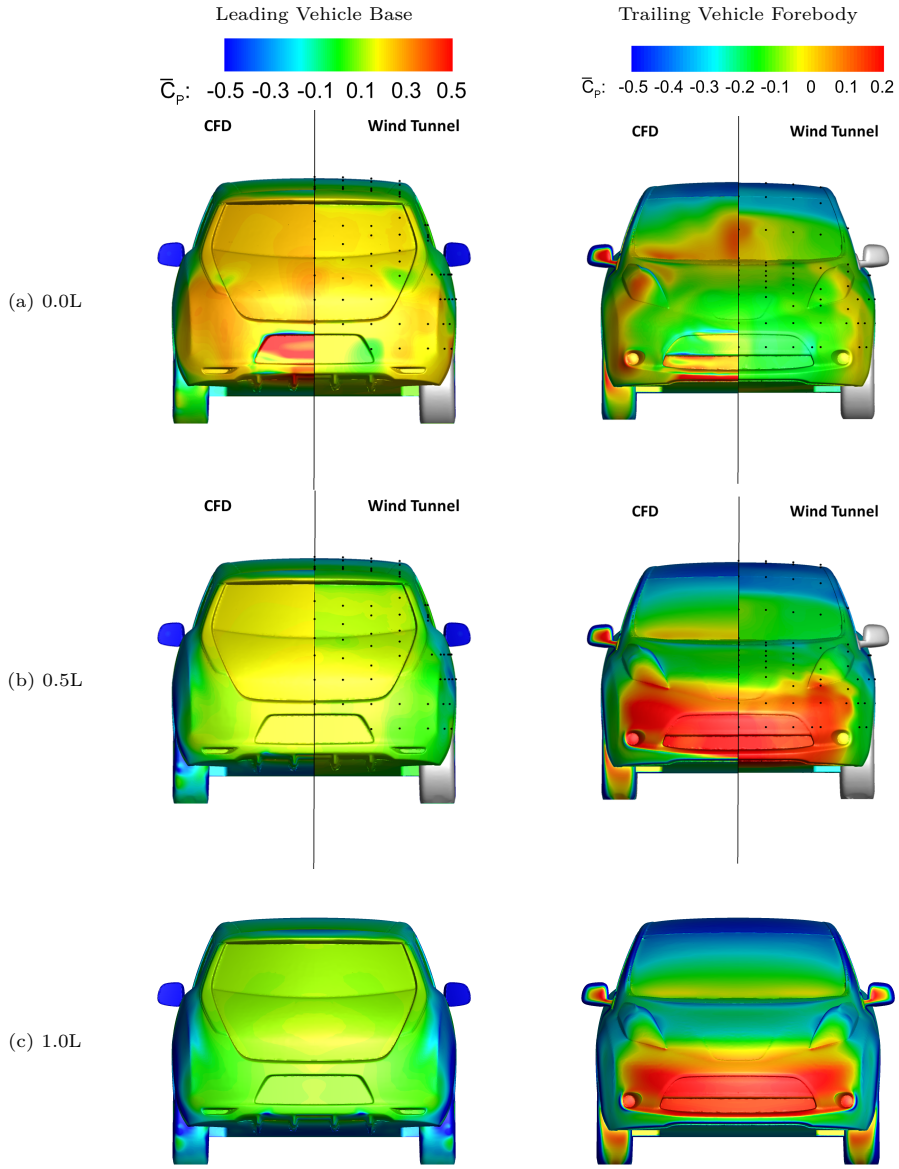

Figure 7: Surface pressure coefficient comparison between the wind tunnel measurements and CFD results for a 2-vehicle platoon at $0.0L$ in (a) and $0.5L$ in (b) and CFD results alone of $1.0L$ spacing in (c)

Examination of the wake structure of the leading vehicle on the $^x/_L = -0.055$ cross-sectional plane for various platoon spacings shown in Figure 8(a) reveals a considerable change in the near-wake detachment in comparison to vehicle-in-isolation. The wake outer features appeared to have "stretched" both laterally along the vehicle span and vertically, which induced a larger separation. For the $0.0L$ spacing, the C-pillar vortices, V1, were suppressed and the inner features of the wake (i.e. the distance between the central cores of the vortices) reduced in lateral length by approximately $^x/_L = \pm 0.04$. With increased spacing, the inner line along with the C-pillar vortices recover in length and position respectively to the vehicle-in-isolation case as the spacing increases to $1.0L$. This change in size remains the most visible modification observed in the wake topology in platoon and continues to influence the wake downstream of the model. The span-wise increment of the wake correlates directly with the pressure increase observed on the leading vehicle upper portion of the base that takes on a similar shape. In all tested spacings, the counter-rotating vortex positions generated behind the wheels, V2, were unaffected by the presence of a trailing vehicle.

The approaching flow from the leading vehicle to the trailing vehicle forebody in Figure 8(b) was modified significantly for $0.0L$ spacing. The three vortical structures convected by the leading model including the A-pillars, V3, C-pillars, V1 and base longitudinal vortices, V4, appear on the trailing vehicle bonnet. The C-pillars and base vortices both impinge on the windscreen rotating in opposite directions and create a unique vortex closure line that correlates with the high pressure zone acting on the trailing model windscreen seen in Figure 7(a). These vortices are only visible for $0.0L$ spacing as the flow separation of the leading vehicle directly

impinges on the trailing vehicle. For larger spacings, these vortical structures breakdown and weaken before reaching the investigated plane of $^{x}/_{L} = -0.887$. However, the convected dissipated and diffused flow from the leading vehicle has far reaching effect that can influence the pressure acting on the bonnet, A-pillars and roof up to $1.0L$ spacing. As the flow separates behind the trailing vehicle, the C-pillar vortex core positions and closure line nearly superimpose to the isolated case as shown in Figure 8(c). This indicates that the wake structure is similar to the isolated case, although trivial difference in base pressure occur on the trailing model that are attributed to the flow dissipation and momentum loss.

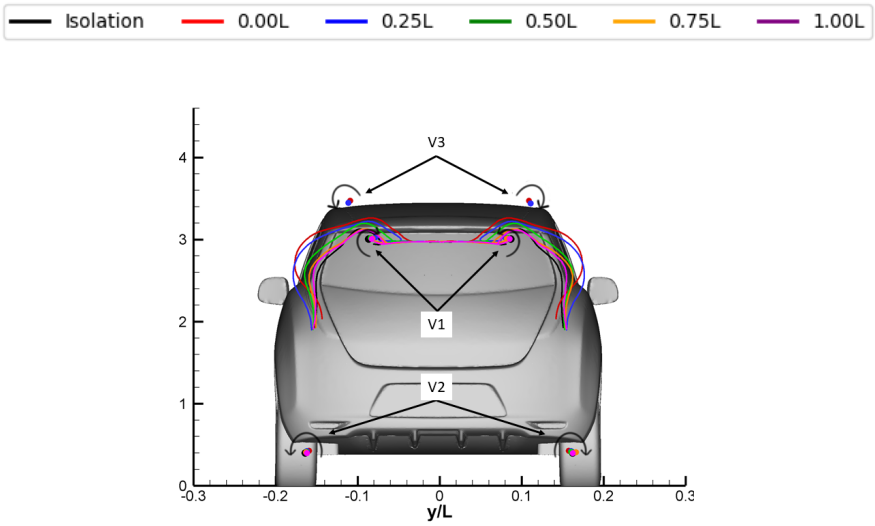

(a) Leading Model Base at $^{x}/_{L} = -0.055$

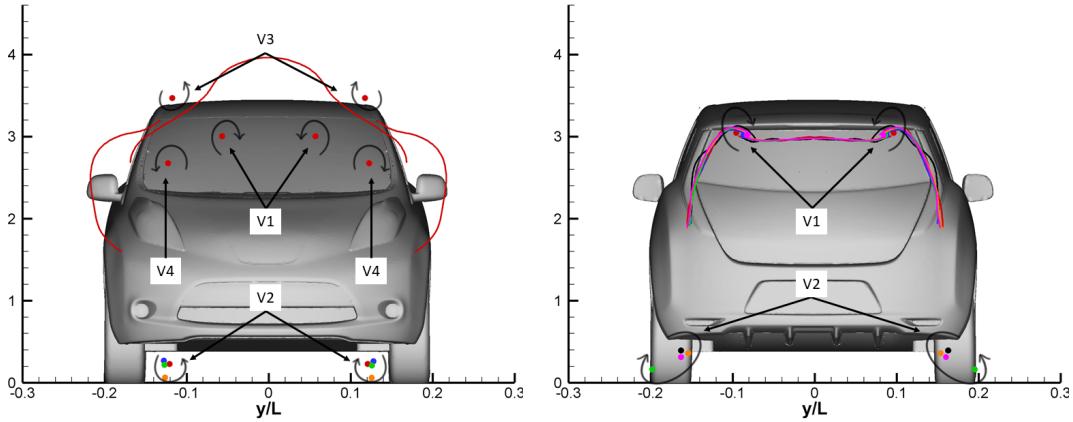

(b) Trailing Model Forebody at $^{x}/_{L} = -0.887$ (c) Trailing Model Base at $^{x}/_{L} = -0.055$

Figure 8: Reconstruction of the CFD results of the in-plane components of velocity streamlines for the leading model base (a), the trailing model forebody (b) and base (c) in a 2-vehicle platoon

Figure 9 shows the velocity magnitudes and in-plane streamlines of the centreline $y/L = 0$ and the horizontal $z/L = 0.144$ planes. It is clear that the longitudinal upper recirculation zone of the leading model base impinges on the trailing model bonnet with the upper free-shear layer impinging on the windscreen centreline creating a zone of high pressure for $0.0L$ spacing (Figure 9(a)) similar to observations of smoke visualisation by Abdel Azim and Abdel Gawad (2000) on notchback vehicles in platoon. When visualised through the horizontal plane, two recirculating vortices are seen to be trapped between the vehicles (similar to a cavity) and only allow the fast moving flow of the leading model sides to impinge on the trailing vehicle side fenders. This verifies the vertical pressure increase along the front side fenders up to the headlights. In addition, the flow at this spacing suppresses the formation of the bottom roll-up vortex of the leading model, hence the significant increase in pressure on the number plate seen in Figure 7(a).

As the platoon spacing increases the flow diffusion of the leading vehicle underbody and the sharp rear tapers (seen in Figure 9) channel the flow inboard causing it to impinge on the trailing vehicle bumper. This clarifies the span-wise increase of the acting pressure for $0.5L$ and $1.0L$ spacings. In addition, the up-washed motion of the flow from the diffuser decreases the flow directed towards the following vehicle underbody. This may induce detrimental effects on the following vehicle(s) stability characteristics particularly on the lift force and pitching moment.

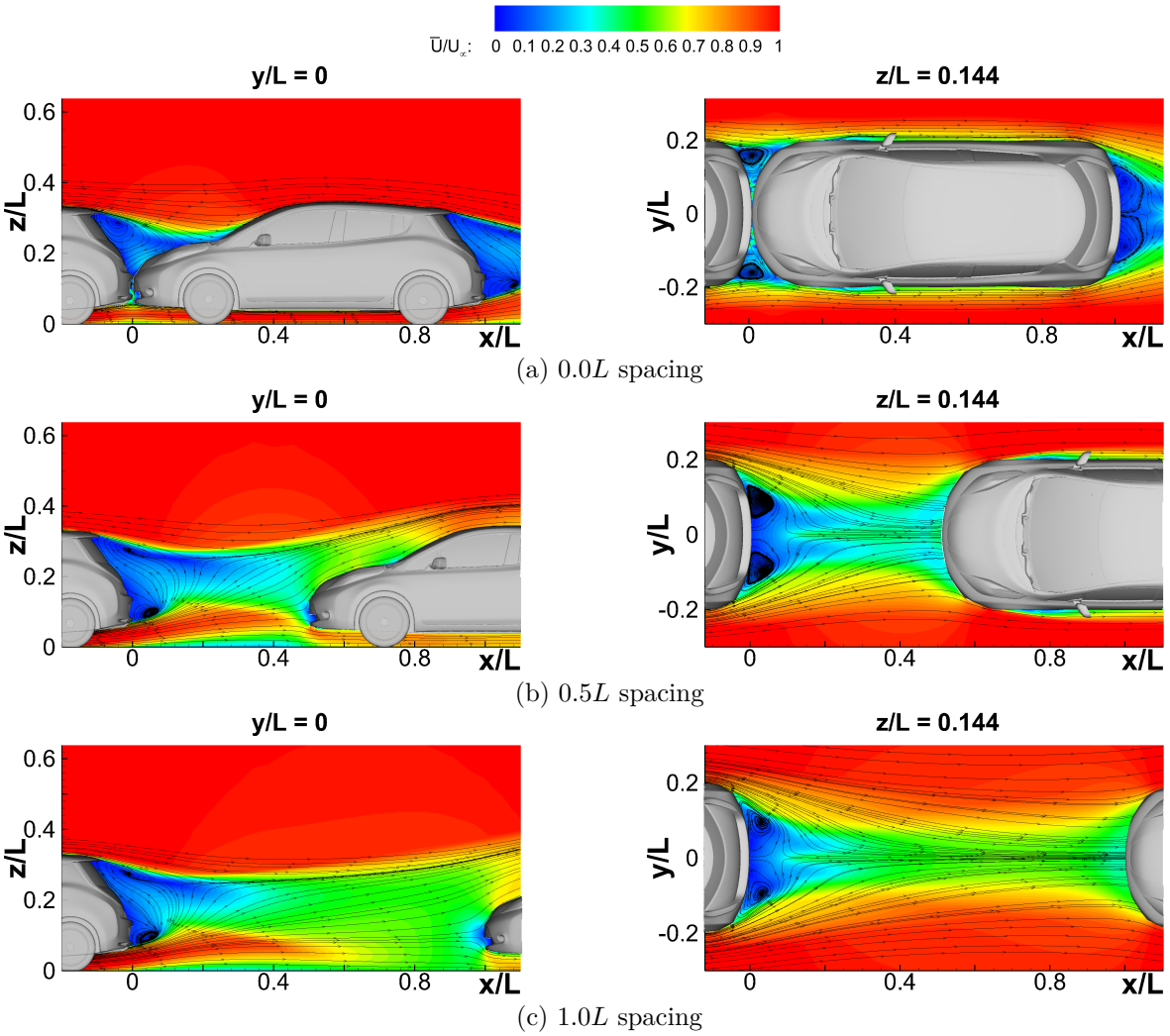

(a) $0.0L$ spacing

(b) $0.5L$ spacing

(c) $1.0L$ spacing

Figure 9: Velocity fields of a 2-vehicle platoon at various platoon spacings for $y/L = 0$ and $z/L = 0.144$ with streamlines of the in-plane velocity components

These flow trajectories and dynamics are ideal to interpret the surface pressure trends, although this method remains limited as it does not offer any quantifiable explanation to the reduction in drag at specific regions. In addition, interpreting the pressure qualitatively may yield misleading conclusions, as although the highest magnitude of pressure seems lower than isolation as previously suggested by Tsuei and Savaş (2001), the overall acting area is higher. Therefore, to precisely identify the region of the vehicle that contributed to drag reduction, the vehicle geometry was split in half as illustrated in Figure 10. The pressure acting on each half was used to calculate the drag contribution to distinguish whether the drag reduction was a result of changes in forebody

or base pressures and aid in the drag interpretation.

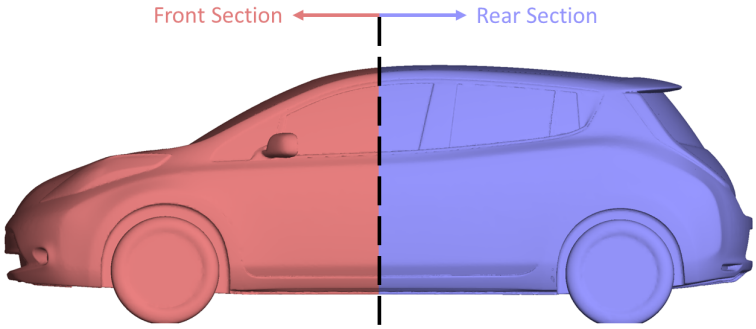

Figure 10: The Nissan Leaf geometry split in half to isolate the drag contribution of the front and rear sections

The differences in absolute pressure magnitudes between the CFD and wind tunnel are quantified in the drag measurements reported in Figure 11(a). Note that these drag measurements are based on the total drag of the vehicle. Evidently, the over-prediction of acting pressure seen in CFD, resulted in higher force measurements for both models in the platoon, although, both methods showed a rather similar trend in drag coefficient. They indicated that with increased spacing the leading vehicle drag increases linearly and remains below an isolated case even at $1.0L$ spacing. This reduction in drag is shown to be a consequence of the base pressure increase as demonstrated in Figure 11(c) by the significant reduction in drag along the base. While the trailing vehicle drag ratio reaches a maximum (above vehicle-in-isolation) at $0.25L$ spacing and drops as the spacing increases, verified by the unfavourable pressure increase acting on the forebody in Figure 11(b). Experimentally, the drag coefficient of the trailing model was characterised with high fluctuations influenced by the flow impingement of the leading model. Despite that, in the majority of the spacings tested, the drag remained comparable to the CFD measurements and showed an increase from the isolated case for the $0.25L$.

The deviations in drag measurements between CFD and wind tunnel measurements were attributed to the differences between the setups of the wind tunnel and simulation environment rather than the performance of the RANS model employed. For the wind tunnel investigations the models had a minor vertical offset to prevent the force balance from bridging onto the ground surface of the wind tunnel. This in combination with the overhead strut and blockage effects that were not corrected for resulted in deviations in the force measurements. Standard deviations obtained from the wind tunnel measurements were also high, which allude to the instability of the flow and dynamic response of the force balance.

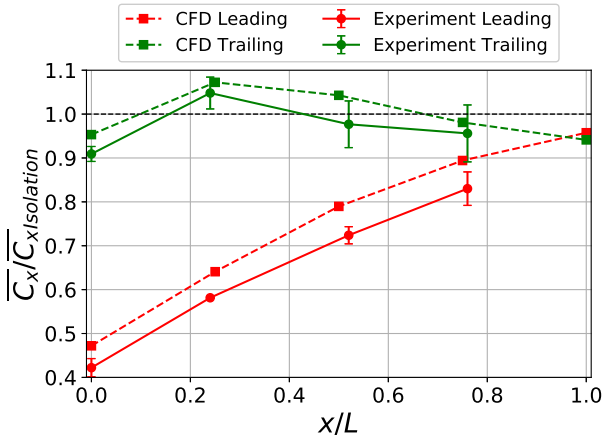

(a) C_X Comparison

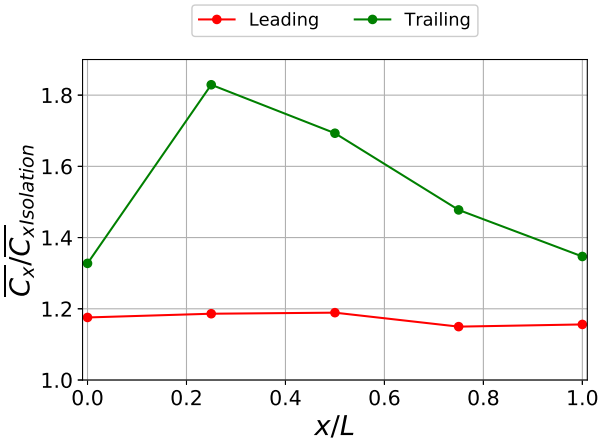

(b) Front Section

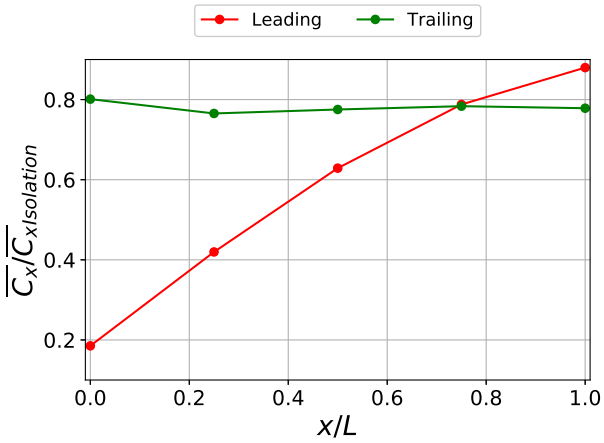

(c) Base Section

Figure 11: The drag coefficient C_X compared between wind tunnel measurement and CFD in (a) for a 2-vehicle platoon. The contribution of the drag broken into the front and rear sections in (b) and (c) respectively

3.3 3-Vehicle platoon

Figure 12 shows the reconstructed velocity streamlines with the main flow features emphasised.

Increasing the number of vehicles in platoon from two to three has indistinguishable effect on the downstream flow-field topology of the leading model (Figure 12(a)). It remains stretched both laterally and vertically with reduced platoon spacing and the appearance of the C-pillar vortices, V1. Similarly, the vortices generated behind the rear wheel wells, V2 are clustered around the same region behind the rear wheels. The leading vehicle wake approaching the middle vehicle takes on a similar structure to that seen in a 2-vehicle platoon (Figure 12(b)), with the C-pillar vortices V1 rotating inboard, whilst the A-pillar, V3 and main longitudinal vortex, V4 rotating in an outboard fashion only for the $0.0L$ spacing case. As the flow separates behind the middle vehicle, it resembles that of the leading vehicle, however with vertical stretching alone. This variation is attributed to the flow dissipation that results in lower flow velocities separating off the model and the large leading vehicle vortex that is channelled to the side of the middle model. A distinct increase in C-pillar vortex (V1) radius was observed for $0.0L$ spacing in Figure 12(c) as it draws the dissipated leading model C-pillar vortices. This low energy wake is convected downstream towards the trailing vehicle, which exhibits directional changes as reported in Figure 12(d). The main (V4) and C-pillar vortices (V1) align perpendicularly spinning in opposite directions, with the flow impingement confined to the car windscreen. External to the car geometry, a large vortex V5 spins parallel to the A-pillars originated from the middle vehicle main vortex. This flow topology is exclusive to $0.0L$ platoon spacing and in all other spacings these structures breakdown before reaching the plane of investigation (i.e. $^x/_L = -0.887$) of the following vehicles. In addition, both the middle and trailing vehicles show that the oncoming flow close to the ground contains a spinning vortex, V2, from the upstream vehicle rear wheel well separation. Finally, the flow separating off the trailing vehicle in Figure 12(e) indicates a similar behaviour to the trailing vehicle of a 2-vehicle platoon with the majority of the wake closure lines and vortex cores superimposing to the vehicle-in-isolation case with minor deviations.

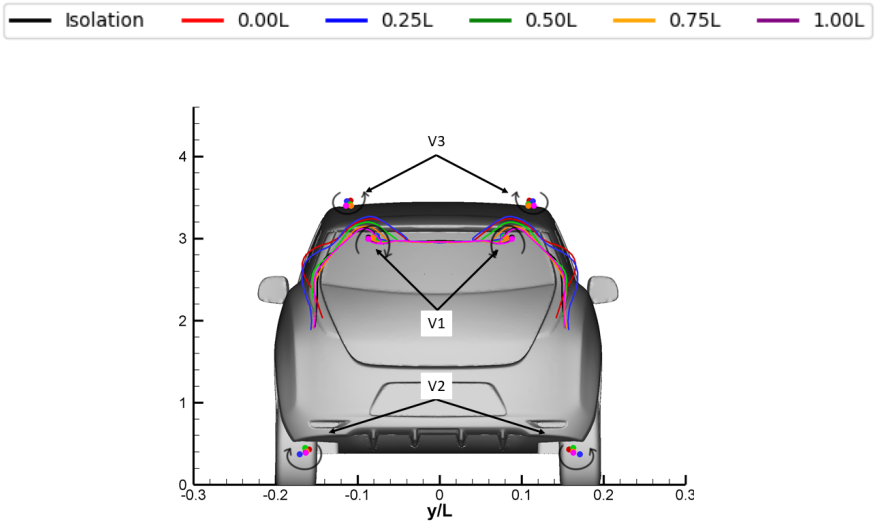

(a) Leading Model Base

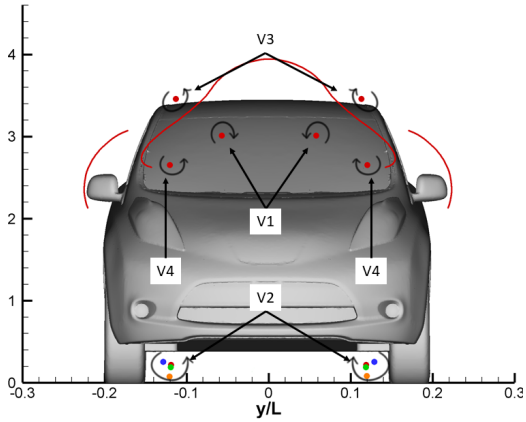

(b) Middle Model Forebody

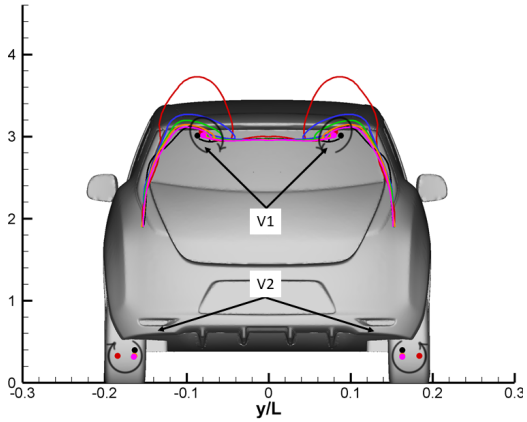

(c) Middle Model Base

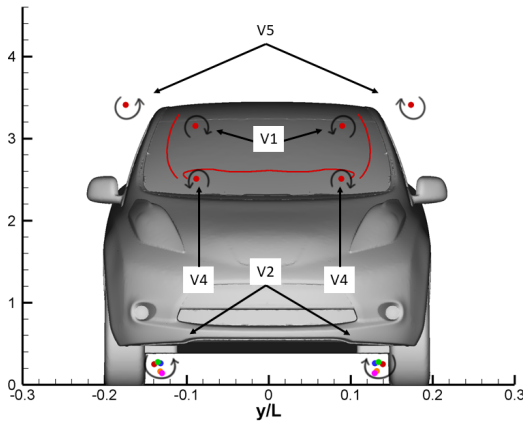

(d) Trailing Model Forebody

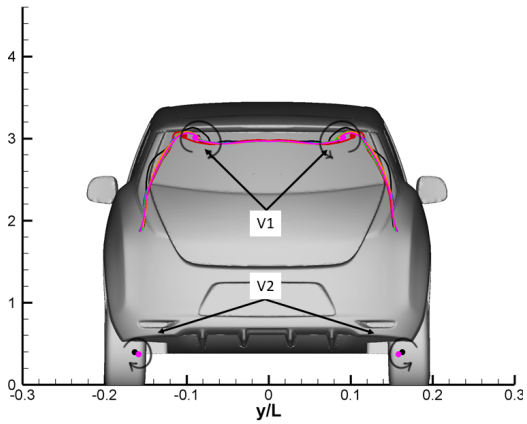

(e) Trailing Model Base

Figure 12: Reconstruction of the CFD results of the in-plane components of velocity streamlines for the leading model base (a), the middle model forebody (b) and base (c) and the trailing model forebody (d) and base (e) in a 3-vehicle platoon

The pressure distribution acting on the leading vehicle base, middle vehicle forebody and the trailing vehicle base reported in Figure 13 is remarkably similar to that observed in a 2-vehicle platoon. No fundamental change occurred to the three-dimensional wake structures observed in those regions as examined in Figure 12.

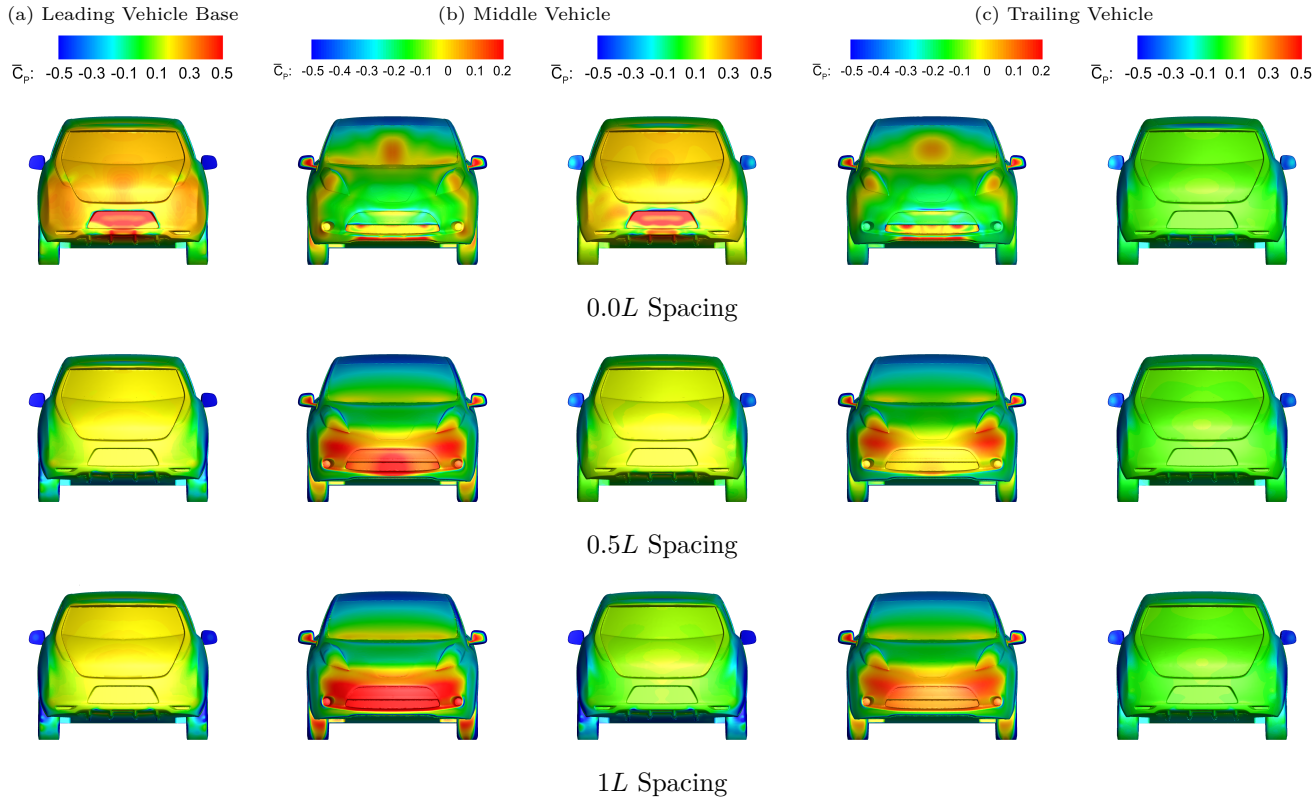

Figure 13: Surface pressure coefficient for a 3-vehicle platoon at three spacings including 0.0L, 0.5L and 1L for the leading vehicle base (a) the middle vehicle (b) and the trailing vehicle (c)

However, the separated flow of the middle vehicle demonstrated changes from the leading vehicle mainly due to the flow dissipation that is clearly reflected in the base pressure loss (Figure 13(b)). Firstly, the wake was elongated in a streamwise direction for all spacings with the closure point (for spacings higher than 0.0L) moving further downstream due to the vertical alignment of the vortex cores seen in Figure 14(b) and (c). This decreased the strength of the flow impingement along the central part of the base and in combination with the reduced near-wake width (Figure 12(c)) caused a pressure drop across the central and upper section of the base surface. The flow impinging onto the trailing vehicle, although modified, has little effect on the trailing vehicle pressure map trend as seen in Figure 13(c) in comparison to the middle vehicle. The regions influenced by the flow impingement at different platoon spacings are consistent and correlate with the velocity streamline directions as demonstrated by Figures 14. The magnitude deficits in pressure between the middle and trailing vehicles was purely a consequence of the flow dissipation, diffusion and momentum loss.

A direct comparison of the forebody drag contribution between the leading and trailing vehicles of a 2-vehicle platoon and the leading and middle vehicles of a 3-vehicle platoon, indicated very minor differences (Figure 15(b)), whilst the trailing vehicle showed significant drop in drag across the forebody, which suggests that the reduced pressure magnitude acting on that region ultimately reduced the axial force exerted. In addition, Figure 15(c) shows that the middle vehicle rear drag out performs the leading vehicle for all the tested spacings apart from 0.0L. That was largely attributed to the decreased axial force acting on the wheels, wheel wells, rear side fenders and spoiler. This reduction compensates for the pressure increase across the middle vehicle forebody and lead to drag improvements. As for the trailing vehicle, the constant drag force declined in comparison to that seen on the trailing vehicle of a 2-vehicle platoon, which in combination with its reduced forebody drag results in overall drag reductions of up to 20%. Interestingly, the order of the highest drag reduction vehicle reverses above 0.75L spacing indicating that the trailing vehicle exhibits the least drag, followed by the middle and leading vehicles respectively as shown in Figure 15(a). This analogy correlates with the axial force changes along the front and rear halves of the vehicles. Most importantly is that in a platoon of three vehicles, all the cars experience drag reductions across all the platoon spacings tested.

To put these drag changes into perspective, simulations of the vehicle running a repeated NEDC drive cycle show that for an individual car a Cd reduction of 0.01 results in an increase in range of 2.6km and a CO_2 reduction of 1.1gCO_2/km (assuming that the electricity was provided from the grid and was generated with a CO_2 production of 0.542 kg CO_2/kWh and that the grid to battery efficiency was 0.92). However, in platoon all of the vehicles travel at a steady, high speed so the gains are very much greater and approach the simple cubic relationship between power drawn from the battery and platoon velocity.

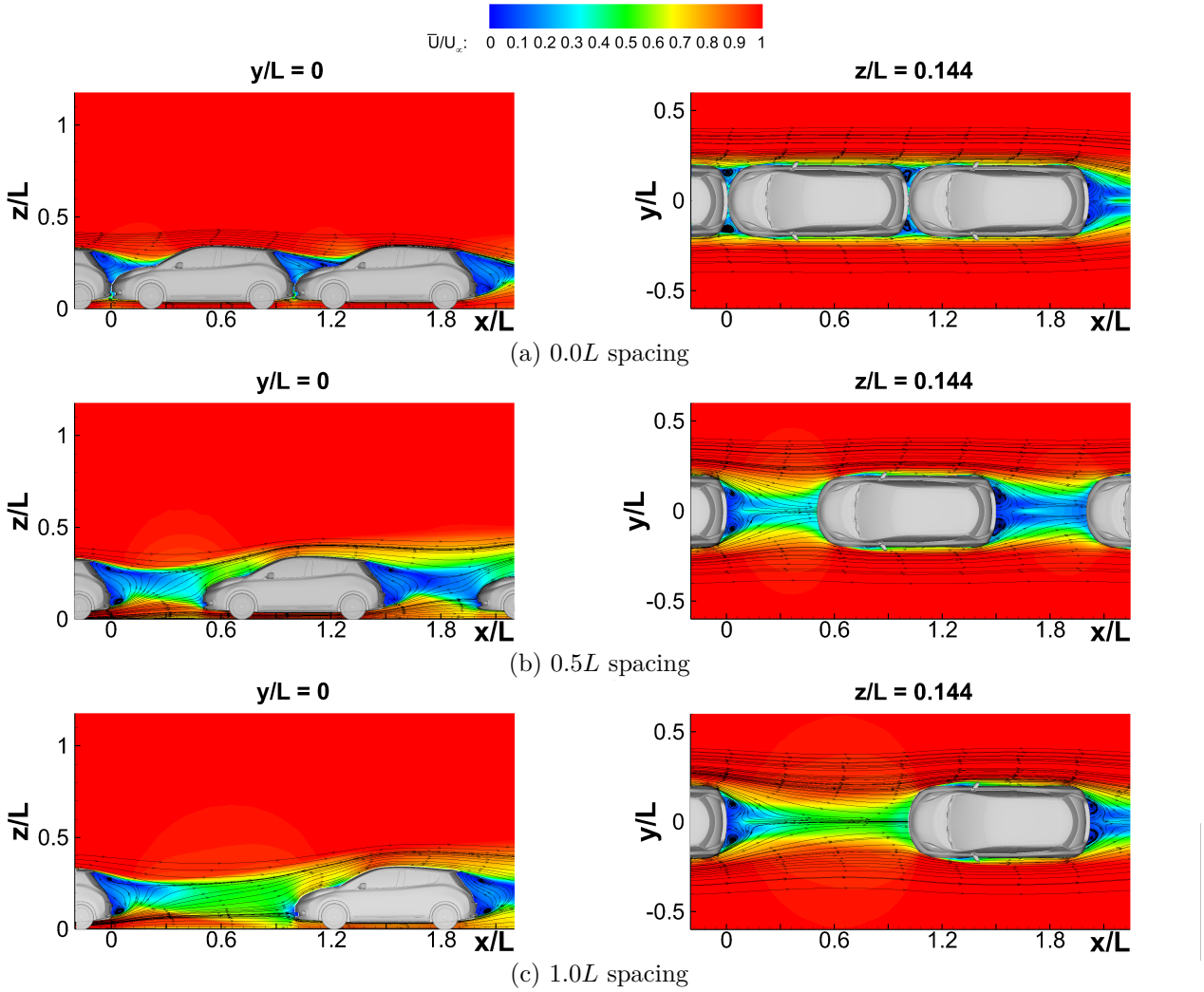

(a) $0.0L$ spacing

(b) $0.5L$ spacing

(c) $1.0L$ spacing

Figure 14: Velocity fields of a 3-vehicle platoon at various platoon spacings for $y/L = 0$ and $z/L = 0.144$ with streamlines of the in-plane velocity components

4 Conclusions

Examination of the aerodynamic performance of individual vehicles in platoon has been investigated using both model wind tunnel measurements and CFD. Force measurements, surface pressure and wake topologies have been discussed for a single Nissan leaf and for two and three vehicles in platoon.

In a 2-vehicle platoon, the drag reduction of the leading vehicle was attributed to the base pressure increase predominantly caused by span-wise and vertical stretching of the near-wake structure. This effect acted in combination with the displacement of the velocity streamlines on the horizontal and centreline planes that are modified by the presence of a trailing vehicle. The pressure field acting on the trailing vehicle was significantly influenced by the flow trajectory of the leading vehicle. Some of the base features that are optimised to minimise the drag of the vehicle-in-isolation such as tapering the sides and adding a diffuser, have a detrimental effect on the following cars, as the impinging flow causes the drag to exceed the vehicle-in-isolation case for $0.25L$ and $0.5L$ spacings. This impingement effect reduces as the spacing increases to the trailing vehicle and the system achieves overall drag reductions largely due to the decrease of the leading model base drag. It also occurs at the expense of the trailing vehicle having higher forebody drag if the spacing is not well optimised.

Increasing the number of vehicles in platoon does not influence the wake between the leading and middle vehicles as the flow interaction remains fundamentally similar to a 2-vehicle platoon. The wake structure of the middle vehicle was modified and only showed signs of vertical stretching, which resulted in a pressure drop in comparison to the leading vehicle. However, the results still indicated that the middle vehicle base drag was lower than the leading vehicle due to the decreased axial force acting on areas such as the wheels, wheel wells, rear side fenders and spoiler. This dissipated low energy flow separated of the middle vehicle also altered the wake approaching the trailing vehicle, minimising the impact of the flow impingement on the forebody and allowing the trailing vehicle forebody drag to reduce by approximately 20% in comparison to the leading vehicle.

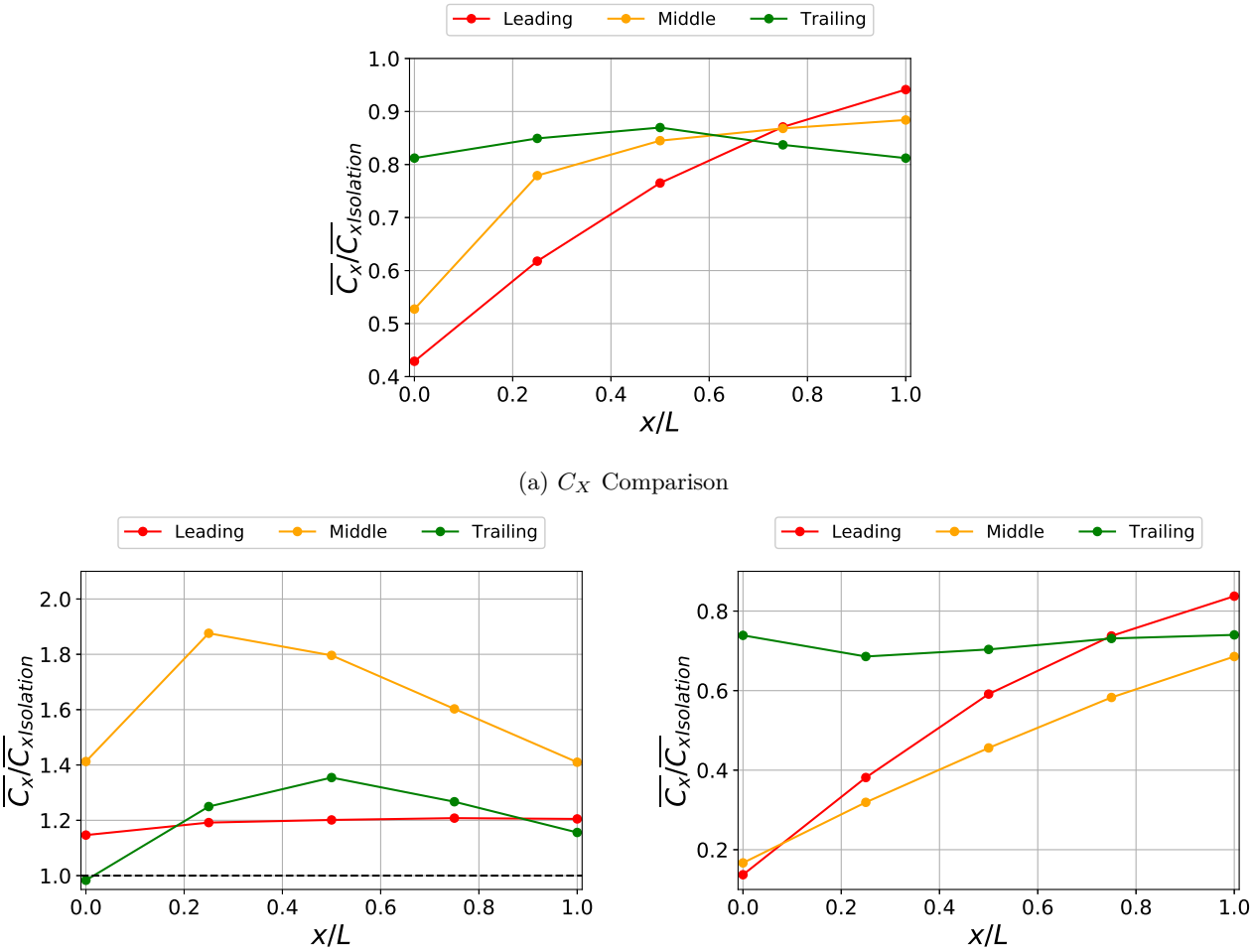

(a) C_X Comparison

(b) Front Section

(c) Base Section

Figure 15: The drag coefficient C_X obtained from CFD in (a) for a 3-vehicle platoon. The contribution of the drag broken into the front and rear sections in (b) and (c) respectively

In such a platoon configuration, all the vehicles experience a drag reduction as the overall magnitude of drag force dropped as a consequence of the reduced impingement energy exerted on the following vehicles.

From these results, the flow physics leading to the drag reductions of individual vehicles in platoon were demonstrated and explained and it has been shown that design features that were optimised for vehicles-in-isolation can have unfavourable effects on the performance of the platoon. It may also be concluded that the sensitivity of the platoon drag to the wake structure of the isolated vehicle may explain the sometimes contradictory conclusions of different investigations.

5 Acknowledgements

The authors would like to acknowledge the support of Nissan Technical Centre Europe for manufacturing the wind tunnel models. Thanks are also due to Mr. Martin Purvis, for keeping the test facility in optimal conditions and Dr. Nicholas Martin for his assistance and guidance in writing the wind tunnel software.

References

Abdel Azim, Ahmed F. and Ahmed F. Abdel Gawad (2000). "A Flow Visualization Study of the Aerodynamic Interference Between Passenger Cars". In: DOI: 10.4271/2000-01-0355. URL: https://www.sae.org/content/2000-01-0355/.

Altinisik, Armagan, Onur Yemenici, and Habib Umur (2015). "Aerodynamic Analysis of a Passenger Car at Yaw Angle and Two-Vehicle Platoon". In: Journal of Fluids Engineering 137.12, p. 121107. ISSN: 0098-2202. DOI: 10.1115/1.4030869. URL: http://fluidsengineering.asmedigitalcollection.asme.org/article.aspx?doi=10.1115/1.4030869.

Axerio, John et al. (2009). "Computational and Experimental Investigation of the Flow Structure and Vortex Dynamics in the Wake of a Formula 1 Tire". In: DOI: 10.4271/2009-01-0775. URL: https://www.sae.org/content/2009-01-0775/.

Beves, Christopher and Stephen. Ferguson (2017). Analysing the aerodynamics of the fastest ever marathon. URL: https://www.theengineer.co.uk/analysing-the-aerodynamics-of-the-fastest-ever-marathon/ (visited on 12/09/2019).

Blocken, Bert, Yasin Toparlar, and Thomas Andrianne (2016). "Aerodynamic benefit for a cyclist by a following motorcycle". In: Journal of Wind Engineering and Industrial Aerodynamics 155, pp. 1–10. ISSN: 01676105. DOI: 10.1016/j.jweia.2016.04.008. URL: https://linkinghub.elsevier.com/retrieve/pii/S0167610516302306.

Blocken, Bert et al. (2018). "Aerodynamic drag in cycling team time trials". In: Journal of Wind Engineering and Industrial Aerodynamics 182, pp. 128–145. ISSN: 01676105. DOI: 10.1016/j.jweia.2018.09.015. URL: https://linkinghub.elsevier.com/retrieve/pii/S0167610518306755.

Bordei, Ștefan and Florin Popescu (2011). "Aerodynamic results for a notchback race car". In: The Annals of "Dunarea de Jos" University of Galati, Fascicle V, Technologies in machine building 29.2 SE - Articles. URL: http://www.gup.ugal.ro/ugaljournals/index.php/tmb/article/view/1796.

Browand, F and M Hammache (2004). "The Limits of Drag Behavior for Two Bluff Bodies in Tandem". In: SAE, Technical Paper Series. SAE International. DOI: 10.4271/2004-01-1145. URL: http://papers.sae.org/2004-01-1145/.

Bruneau, Charles-Henri, Khodor Khadra, and Iraj Mortazavi (2017). "Flow analysis of square-back simplified vehicles in platoon". In: International Journal of Heat and Fluid Flow 66, pp. 43–59. ISSN: 0142727X. DOI: 10.1016/j.ijheatfluidflow.2017.05.008. URL: https://linkinghub.elsevier.com/retrieve/pii/S0142727X16306270.

Bull, M.K. et al. (1996). "Interaction between a vortex wake and an immersed rectangular plate". In: Experimental Thermal and Fluid Science 12.2, pp. 209–220. ISSN: 08941777. DOI: 10.1016/0894-1777(95)00099-2. URL: https://linkinghub.elsevier.com/retrieve/pii/0894177795000992.

Dabnichki, Peter and Eldad Avital (2006). "Influence of the postion of crew members on aerodynamics performance of two-man bobsleigh". In: Journal of Biomechanics 39.15, pp. 2733–2742. ISSN: 00219290. DOI: 10.1016/j.jbiomech.2005.10.011. URL: https://linkinghub.elsevier.com/retrieve/pii/S0021929005004550.

Davila, Arturo et al. (2013). "Environmental Benefits of Vehicle Platooning". In: DOI: 10.4271/2013-26-0142. URL: https://www.sae.org/content/2013-26-0142/.

Ebrahim, Hesham (2019). "The Aerodynamic Characteristics of Passenger Vehicles Operating in a Platoon". PhD thesis. Northumbria University, pp. 70–81.

Ebrahim, Hesham M., Robert G. Dominy, and Pak S. Leung (2016). "Evaluation of vehicle platooning aerodynamics using bluff body wake generators and CFD". In: 2016 International Conference for Students on Applied Engineering (ISCAE). IEEE, pp. 218–223. DOI: 10.1109/ICSAE.2016.7810191. URL: http://ieeexplore.ieee.org/document/7810191/.

Fu, Chen et al. (2017). "Turbulence Models and Model Closure Coefficients Sensitivity of NASCAR Racecar RANS CFD Aerodynamic Predictions". In: SAE International Journal of Passenger Cars - Mechanical Systems 10.1, pp. 2017–01–1547. ISSN: 1946-4002. DOI: 10.4271/2017-01-1547. URL: https://www.sae.org/content/2017-01-1547/.

Georgiadis, Nicholas and Dennis Yoder (2013). "Recalibration of the Shear Stress Transport Model to Improve Calculation of Shock Separated Flows". In: 51st AIAA Aerospace Sciences Meeting including the New Horizons Forum and Aerospace Exposition. Reston, Virigina: American Institute of Aeronautics and Astronautics. ISBN: 978-1-62410-181-6. DOI: 10.2514/6.2013-685. URL: http://arc.aiaa.org/doi/10.2514/6.2013-685.

Gheyssens, Thomas and Gandert Van Raemdonck (2016). "Effect of the Frontal Edge Radius in a Platoon of Bluff Bodies". In: SAE International Journal of Commercial Vehicles 9.2, pp. 2016–01–8149. DOI: 10.4271/2016-01-8149. URL: https://www.sae.org/content/2016-01-8149/.

He, Mingzhe et al. (2019). "Detached eddy simulation of a closely running lorry platoon". In: Journal of Wind Engineering and Industrial Aerodynamics 193, p. 103956. ISSN: 01676105. DOI: 10.1016/j.jweia.2019.103956. URL: https://linkinghub.elsevier.com/retrieve/pii/S0167610519305471.

Jacuzzi, Eric and Kenneth Granlund (2019). "Passive flow control for drag reduction in vehicle platoons". In: Journal of Wind Engineering and Industrial Aerodynamics 189, pp. 104–117. ISSN: 01676105. DOI: 10.1016/j.jweia.2019.03.001. URL: https://linkinghub.elsevier.com/retrieve/pii/S0167610518309474.

Koenig, Keith and Anatol Roshko (1985). “An experimental study of geometrical effects on the drag and flow field of two bluff bodies separated by a gap”. In: Journal of Fluid Mechanics 156.-1, p. 167. ISSN: 0022-1120. DOI: 10.1017/S002211208500204X. URL: http://www.journals.cambridge.org/abstract{_}S002211208500204X.

Le Good, Geoffrey et al. (2019). “An Investigation of Aerodynamic Characteristics of Three Bluff Bodies in Close Longitudinal Proximity”. In: SAE International. DOI: 10.4271/2019-01-0659. URL: https://www.sae.org/content/2019-01-0659/.

Ljungkrona, Lars and Bengt Sundén (1993). “Flow visualization and surface pressure measurement on two tubes in an inline arrangement”. In: Experimental Thermal and Fluid Science 6.1, pp. 15–27. ISSN: 08941777. DOI: 10.1016/0894-1777(93)90037-J. URL: https://linkinghub.elsevier.com/retrieve/pii/089417779390037J.

Maleki, Siavash, David Burton, and Mark C. Thompson (2017). “Assessment of various turbulence models (ELES, SAS, URANS and RANS) for predicting the aerodynamics of freight train container wagons”. In: Journal of Wind Engineering and Industrial Aerodynamics 170, pp. 68–80. ISSN: 01676105. DOI: 10.1016/j.jweia.2017.07.008. URL: https://linkinghub.elsevier.com/retrieve/pii/S0167610517302921.

Mercker, Edzard and Jochen Wiedemann (1996). “On the Correction of Interference Effects in Open Jet Wind Tunnels”. In: DOI: 10.4271/960671. URL: https://www.sae.org/content/960671/.

Morel, T. and M. Bohn (1980). “Flow Over Two Circular Disks in Tandem”. In: Journal of Fluids Engineering 102.1, pp. 104–111. ISSN: 0098-2202. DOI: 10.1115/1.3240599. URL: https://asmedigitalcollection.asme.org/fluidsengineering/article/102/1/104/426913/Flow-Over-Two-Circular-Disks-in-Tandem.

Nakada, Tohru, Shigeaki Ishikawa, and Shunji Oki (2014). “Development of an Electric Motor for a Newly Developed Electric Vehicle”. In: DOI: 10.4271/2014-01-1879. URL: https://www.sae.org/content/2014-01-1879/.

Pagliarella, Riccardo M, Simon Watkins, and Angelo Tempia (2007). “Aerodynamic Performance of Vehicles in Platoons: The Influence of Backlight Angles”. In: SAE, Technical Paper Series. SAE International. ISBN: 0148-7191. DOI: 10.4271/2007-01-1547. URL: http://papers.sae.org/2007-01-1547/.

Saunders, J.W., S. Watkins, and R.J. Cassar (1993). “Vortex optimisation of slotted tops and cavities of two different open rail wagons”. In: Journal of Wind Engineering and Industrial Aerodynamics 49.1-3, pp. 421–430. ISSN: 01676105. DOI: 10.1016/0167-6105(93)90036-N. URL: https://linkinghub.elsevier.com/retrieve/pii/016761059390036N.

Schito, Paolo and Francesco Braghin (2012). “Numerical and Experimental Investigation on Vehicles in Platoon”. In: SAE International Journal of Commercial Vehicles 5.1, pp. 2012–01–0175. ISSN: 1946-3928. DOI: 10.4271/2012-01-0175. URL: http://papers.sae.org/2012-01-0175/.

Soares, Renan F., Kevin P. Garry, and Jennifer Holt (2017). “Comparison of the Far-Field Aerodynamic Wake Development for Three DrivAer Model Configurations using a Cost-Effective RANS Simulation”. In: DOI: 10.4271/2017-01-1514. URL: https://www.sae.org/content/2017-01-1514/.

Tsuei, Lun and Ömer Savaş (2001). “Transient aerodynamics of vehicle platoons during in-line oscillations”. In: Journal of Wind Engineering and Industrial Aerodynamics 89.13, pp. 1085–1111. ISSN: 01676105. DOI: 10.1016/S0167-6105(01)00073-3. URL: https://linkinghub.elsevier.com/retrieve/pii/S0167610501000733.

Watkins, Simon and Gioacchino Vino (2008). “The effect of vehicle spacing on the aerodynamics of a representative car shape”. In: Journal of Wind Engineering and Industrial Aerodynamics 96.6-7, pp. 1232–1239. DOI: 10.1016/j.jweia.2007.06.042. URL: https://linkinghub.elsevier.com/retrieve/pii/S0167610507001687.

Zabat, Michael et al. (1995). “Drag Forces Experienced by 2, 3 and 4-Vehicle Platoons at Close Spacings”. In: SAE, Technical Paper Series. SAE International. DOI: 10.4271/950632. URL: http://papers.sae.org/950632/.